Grapevine stilbenoids as natural food preservatives: calorimetric and spectroscopic insights on the interaction with model cell membranes

Francesca Saitta[1,§], Stefania Mazzini[1,§], Luce Mattio[1], Marco Signorelli[1], Sabrina Dallavalle[1], Andrea Pinto[1,*] and Dimitrios Fessas[1,*]

[1]Dipartimento di Scienze per gli Alimenti, la Nutrizione e l'Ambiente, DeFENS, Università degli Studi di Milano, Via Celoria 2, 20133, Milano, Italy

[§] Authors contributed equally to the research work

*dimitrios,fessas@unimi.it; andrea.pinto@unimi.it

Abstract:

Food contamination with pathogenic microorganisms, such as *Listeria monocytogenes*, *Salmonella enterica*, *Staphylococcus aureus* and *Bacillus cereus*, is a common health concern. Natural product, which have been the main source of antimicrobials for centuries, may represent a turning point in alleviating the antibiotic crisis, and plant polyphenolic compounds are considered a promising source for new antibacterial agents. Resveratrol and resveratrol-derived monomers and oligomers (stilbenoids) have been shown to exert a variegated pattern of efficacies as antimicrobials depending on both the polyphenols' structure and the nature of the microorganisms, and the bacterial cell membrane seems to be one of their primary targets.

In this scenario and basing on the thermodynamic information reported in the literature about cell membranes, this study aimed at the investigation of the direct interaction of selected stilbenoids with a simple but informative model cell membrane. Three complete stilbenoid "monomer / dimer / dehydro-dimer" sets were chosen according to different geometries and substitution patterns. Micro-DSC was performed on 2:3 DPPC:DSPC small unilamellar vesicles with incorporated polyphenols at physiological pH and the results were integrated by complementary NMR data. The study highlighted the molecular determinants and mechanisms involved in the stilbenoid-membrane interaction, and the results were well correlated with the microbiological evidence previously assessed.

Keywords: Stilbenoids; Antimicrobials; Model Membrane; Micro-DSC; NMR.

Introduction

Foodborne diseases caused by pathogens including *Salmonella* sp., *Staphylococcus aureus, Clostridium perfringens, Bacillus cereus, Escherichia coli, Vibrio parahaemolyticus* and *Listeria monocytogenes* have become a major concern for the food industry worldwide.[1,2] In the past years, considerable effort has been made to effectively control the growth of several pathogenic and spoilage microorganisms by combining physical methods and chemical preservatives[3], as well as to reduce the deriving negative effects on food nutritive values, sensory properties and on human health[4].

In this context, several studies have been dedicated to find naturally occurring compounds as effective and safe food-preservative alternatives. In particular, plant polyphenolic compounds have been extensively screened[5]. Among others, stilbenoids represent an attractive class of plant polyphenols studied in the last decades because of their various bioactivities such as anti-inflammatory, neuroprotective, anticancer, antidiabetic effects[6,7], as well as for their antioxidant and antimicrobial properties, which have made them excellent natural food-preservative candidates[8,9].

Stilbenoids are both woody constitutive metabolites and phytoalexins, *i.e.*, molecules produced to protect the plant against biotic and abiotic stresses. Oligostilbenoids are produced by the oligomerization of monomeric units, which generates a large variety of chemotypes, characterized by different connections between aromatic rings, number, type and position of substituents, three-dimensional shape and geometry[10,11].

Grapevine wastes have been reported to be a valuable source of stilbenoids. For instance, up to 41 stilbenes have been identified in grapevine canes, especially in the *Vitis vinifera* genus, in a concentration ranging from 2000 to 6000 mg/kg dry weight.[12] However, huge variability in both their identification and quantification has been observed. Notably cultivar variety, climate conditions, soil and grapevine management affect the stilbene content, as well as different extraction and analysis methods.[13]

Due to the wide pattern of bioactivities shown, grapevine extracts have already found their own applicability in the food sector.[13,14] For instance, the use of a commercially distributed grapevine-shoot stilbene extract (Vineatrol®) as an alternative to SO_2 in winemaking treatments has been studied, revealing its ability to preserve the enological parameters of wines, though the dosage needs to be optimized in order to avoid side effects on sensory properties.[15–17] Similar extracts have also been embedded in biodegradable plastics for packaging in order to limit the action of pathogenic microorganisms and the deterioration process of food.[14,18] Furthermore, extracts from grape pomace have also been introduced in the agricultural field as antifungals, insecticides, nematicides and as bio-stimulants in grapevines.[13,19]

As a consequence of the above reported potentialities, the extraction of *trans*-resveratrol and its oligomers from grapevine (*Vitis vinifera* L.) wastes as roots, stems, and shoots from the viticulture industry has been reported to have an estimated global economic value of >$45 billion.[20,21] Nonetheless, although grapevine sourced monomers (*e.g.*, resveratrol and pterostilbene) have been extensively studied, less information is available about oligostilbenoids.

Recently, we have evaluated the antimicrobial activity of a collection of resveratrol-derived monomers and dimers against a panel of foodborne pathogens.[22] The most promising dimeric compound, dehydro-δ-viniferin, was tested against *Listeria monocytogenes*, resulting in a loss of cultivability, viability, and cell membrane potential. TEM analysis revealed severe morphological modifications on the cell membrane and leakage of intracellular content, suggesting that the membrane might be the principal biological target of the tested derivative. The findings are in good agreement with previous reports about the conformational changes in membrane structure induced by other natural polyphenols.[23]

Nevertheless, the molecular aspects of the stilbenoid-membrane interaction are still missing in the literature and deserve to be addressed to directly assess such an interaction and to highlight peculiarities of each compound. Indeed, previous calorimetric and spectroscopic studies[24–28] revealed that cell membranes may be severely affected by external agents, but the interaction effects are usually peculiar and strongly dependent on the stereochemistry and geometry of the compound.

To fulfil this gap, we investigated the interaction of eight compounds including stilbenoid monomers (resveratrol and pterostilbene), dimers and dehydro-dimers with a model cell membrane to assess the structural and thermodynamic determinants that dictate the membrane stability alterations and to verify whether they may be correlated to the observed antimicrobial activity. In order to perform a systematic study, compounds with different geometry and substitution pattern were chosen as to investigate three complete "monomer / dimer / dehydro-dimer" sets.

Based on previous thermodynamic studies[24–26], the phospholipid composition of the model cell membrane was selected to be simple but informative, *i.e.*, able to discriminate the main contributions of the constituents, together with the effects of the interacting stilbenoids. Specifically, Small Unilamellar Vesicles (SUVs) at 2:3 DPPC:DSPC molar ratio were prepared as model system and the interaction of stilbenoids with the model membrane at a maximum incorporation level was assessed at physiological pH by using the micro-DSC technique. Furthermore, in order to gain further insights on their initial interaction with the membrane's external surface, an investigation of the stilbenoids inclusion process into the hydrophobic portion of the membrane was additionally carried out on some selected compounds, also discriminating the influence of both the molecular geometry and the substitution pattern.

The results achieved through the calorimetric approach were integrated with complementary information by mono- and bidimensional NMR spectroscopy studies on simpler monolayer systems based on SDS micelles.

Materials and methods

Materials

1,2-distearoyl-sn-glycero-3-phosphocholine (DSPC) and 1,2-dipalmitoyl-sn-glycero-3-phosphocholine (DPPC) powders were purchased from Avanti Polar Lipids (purity certified by the supplier >99%) and were used without any further purification, and sodium dodecyl sulphate (SDS), other chemicals and all solvents were obtained from Sigma-Aldrich and were of analytical grade.

All stilbenoids used are numbered and shown in Figure 1. Trans-Resveratrol **1** and pterostilbene **2** were purchased from Sigma-Aldrich (Milan, Italy). Stilbenoids **3-7** were prepared as previously reported in the literature[22]; compound **8** was synthesised as reported in the Supplementary Material. All compounds were stored in darkness at -20°C before use.

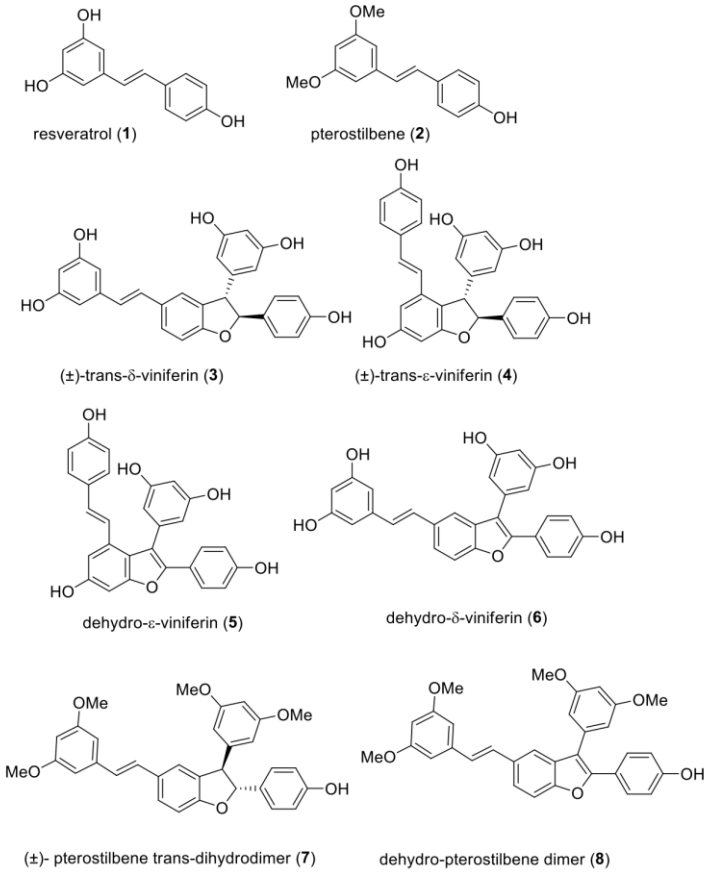

Figure 1. Structures of stilbenoid monomers (**1**,**2**) dimers (**3**,**4**,**7**) and dehydro-dimers (**5**,**6**,**8**).

Liposomes preparation

Liposomes were prepared through thin-film hydration[29]. The phospholipid mixtures for the free liposomes (reference system) were dissolved in chloroform, whereas phospholipids:stilbenoid mixtures (10:1 molar ratio) were dissolved in chloroform:methanol 9:1 in a round-bottomed flask. The mixtures were dried under a stream of dry nitrogen gas and evaporated to dryness through rotary evaporation (Heidolph Laborota 4000 efficient, WB eco, Schwabach, Germany) at 40-45°C. The films were kept under vacuum for at least 3 hours to remove solvent traces and then aged overnight at 4°C. For the hydration, 10 mM phosphate buffer (pH 7.4) at a temperature above the gel-to-liquid-crystal transition of the lipid system was added up to a 10 mg/mL lipid concentration. After the complete dispersion of the lipid films, the obtained mixtures were slowly stirred in water bath, at the same temperature chosen for the buffer, for about an hour until the induction of a homogenous suspension, ensuring to protect samples from light. The Multilamellar Lipid Vesicles (MLVs) dispersions obtained were extruded through polycarbonate filters (pore size of 100 nm) mounted on a heated mini-extruder (Avanti Polar Lipids, Alabaster, AL, USA) fitted with two 1 mL gastight syringes (Hamilton, Reno, NV, USA) in order to obtain suspensions of Small Unilamellar Vesicles (SUVs). An odd number of passages, usually 41, was performed to avoid any contamination by liposomes that might have not passed through the filters, as suggested elsewhere[30].

According to a previous study[26], we demonstrated that the protocol applied for the SUVs preparation produces unilamellar vesicles with a distribution around the nominal provided by the supplier (100 nm), as indicated by dynamic light scattering data. Furthermore, deviations in liposome size and polydispersity are not able to influence the micro-DSC thermograms in the case of multicomponent systems. For this reason, this characterization was not repeated here.

Thermal analysis measurements

Calorimetry was used to determine the thermodynamic stability of the membranes with specific reference to transitions of the lipid phases. Micro-DSC was selected as the most suitable technique for liposome investigation[31]. The instrument used was a Setaram micro DSCIII (Setaram Instrumentation, Caluire, France) operating with 1 mL hermetically closed pans at 0.5 °C/min scanning rate. After the conclusion of the liposomes' preparation protocols, each dispersion was allowed to anneal for at least 30 min at room temperature before launching the DSC measurement. SUVs samples were diluted up to 2.8 mM phospholipid concentration. The phospholipid concentration was derived by accurately considering the lipids weight and the dilution volumes at

each step of the liposome preparation protocol (the validity of such approach was assessed in previous works)[24,26].

The influence of a different phospholipid:stilbenoid ratio (10:2 molar ratio) as well as the role of the steric hindrance given by the compound's molecular size (monomer vs dimer) were also verified by using compounds **1** and **3** (Figure 1) from the first set (see Supplementary Material).

In some specific cases, additional measurements were also performed on samples prepared by adding stilbenoids to the preformed reference liposomes in order to evaluate the process of insertion of the compounds into the phospholipid bilayer. In particular, just before launching the measurement, a volume of 1 μL of highly concentrated stilbenoid solutions in DMSO was added and well mixed with 1 mL of SUVs at 2.8 mM phospholipid concentration, reaching the same lipid:stilbenoid ratio used for the other experiments (10:1 lipid:stilbenoid molar ratio). The influence of the external addition of such a DMSO % v/v was assessed and does not affect the vesicles thermotropic behaviour, as also confirmed by the literature (see Supplementary Material)[32,33].

The raw data were worked out with the dedicated software "THESEUS"[34,35]. Briefly, the apparent specific heat trace, $C_p^{app}(T)$, was scaled to obtain the excess specific heat, $C_p^{exc}(T)$, with respect to the low temperature lipids state. Due to such a treatment, the area beneath the recorded peaks directly corresponds to the relevant transition enthalpy $\Delta H°$ of the lipid phase. Four heating-cooling cycles were applied to the samples to ensure the achievement of stable lipid phases (all cycles heating curves were superimposable unless otherwise indicated). All transitions were reversible, and the second cycle heating curves were respectively considered to evaluate the parameters of the thermotropic transitions observed. Errors were evaluated on the basis of at least three replicas.

In order to quantitatively compare and discuss the DSC data in terms of transition cooperativity between different systems, which are always characterized by complex and multiphasic signals, we adopted the transition average temperature, $\bar{T}$, and the average cooperativity index, *ACI*, defined elsewhere[26]. Briefly, the transition average temperature, $\bar{T}$, is defined as

$$\bar{T} = \int_{T_0}^{T_f} T \cdot f(T) dT$$

being T_0 and T_f the initial and final limit of the observable peak, respectively, and the frequency function $f(T)$ is the normalized calorimetric peak distribution

$$f(T) = \frac{C_p{}^{exc}(T)}{\Delta H°} \ ,$$

whereas the average cooperativity index, *ACI*, is defined as

$$ACI = \sqrt{\int_{T_0}^{T_f} (T - \bar{T})^2 \cdot f(T) dT} \ .$$

Following the ACI definition reported above, which reflects the width of the peak, the higher the ACI value, the lower the cooperativity of the transition. A further detail about the calorimetric profile is the peak asymmetry index, which can be obtained through the $|\bar{T} - T_{max}|$ difference.

NMR spectroscopy

Resveratrol, dehydro-δ-viniferin and (±)-*trans*-ε-viniferin were dissolved in 0.6 mL of SDS (Sodium dodecyl sulphate) in D_2O pH 6.0 to the concentration of 15 mM. The concentration of SDS solution (24.8 mM) was greater than critical micelle concentration (8.2 mM)[36]. SDS micelles are often used as membrane models in NMR spectroscopy[37]. The NMR spectra were carried out at 25°C on a Bruker AV600 spectrometer operating at a frequency of 600.10 MHz, equipped with a z-gradient 5mm TXI probe. Chemical shifts (ppm) were referenced to residual solvent signal at 4.78 ppm. The protons of resveratrol, dehydro-δ-viniferin and (±)-*trans*-ε-viniferin were assigned using an integrated series of 2D experiments such as ROESY, NOESY, COSY and TOCSY. ROESY spectra were recorded with spin-lock of 250 and 400 ms. Phase sensitive NOESY spectra were acquired in TPPI mode, with 2048 x 1024 complex FIDs. Mixing times ranged from 100 ms to 400 ms. TOCSY spectra were acquired with the use of a MLEV-17 spin-lock pulse (60 ms total duration). All spectra were transformed and weighted with a 90° shifted sine-bell squared function to 4K x 4K real data points.

Results and discussion

Differential scanning calorimetry

Cell membrane thermodynamic stability depends on several factors such as size, lipid composition, phospholipid headgroup and tails, unsaturation level, etc. These aspects has been extensively studied and reported in recent works[24–26] starting from simple systems up to fifteen component complex membranes. This systematic dissection of the thermodynamic determinants dictating the cell membrane stability and the assessment of an interaction hierarchy allowed to downgrade the complexity of the system and to design a simple but informative model lipid membrane that highly reproduced the thermodynamic behaviour exhibited by real cell membranes[24].

Nonetheless, this work is not aimed at accurately mimicking the bacterial cell membrane composition, but its purpose is to evaluate the direct interaction of selected stilbenoids (Figure 1) with a phospholipid vesicle expressly designed in order to highlight the forces that drive such an interaction.

With this purpose, we decided to downgrade the complexity of the system at minimum, designing a specific model cell membrane with a simple composition as 2:3 molar ratio of DPPC:DSPC. Specifically, being aware that cell membranes are always characterized by the presence of a certain percentage of unsaturated phospholipids, two saturated phospholipids were purposely chosen for this study. Indeed, in general, both the enthalpic and entropic contributions to the membrane stability provided by saturated phospholipids result to be additive, *i.e.*, simply follows the constituents' proportion[26]. Such a property, which would have been lost in the presence of unsaturated constituents, together with the high simplicity of the system, permits an easier discrimination and interpretation of the interactions observed basing on the knowledge about each thermodynamic contribution to the cell membrane stability. Moreover, the same headgroup (choline) was selected in order to better discriminate the effects of two different tail length (the shortest palmitoyl chain in DPPC and longest stearoyl one in DSPC) seeking the enhancement of the thermodynamic phase separation, already present in a DPPC:DSPC binary system, upon any interaction of the compounds with the hydrophobic portion of the bilayer[26]. Indeed, such an enhancement of the phase separation would magnify any possible preferential interaction of the compounds with specific portions of the bilayer, which might be driven by thermodynamic and/or structural factors.

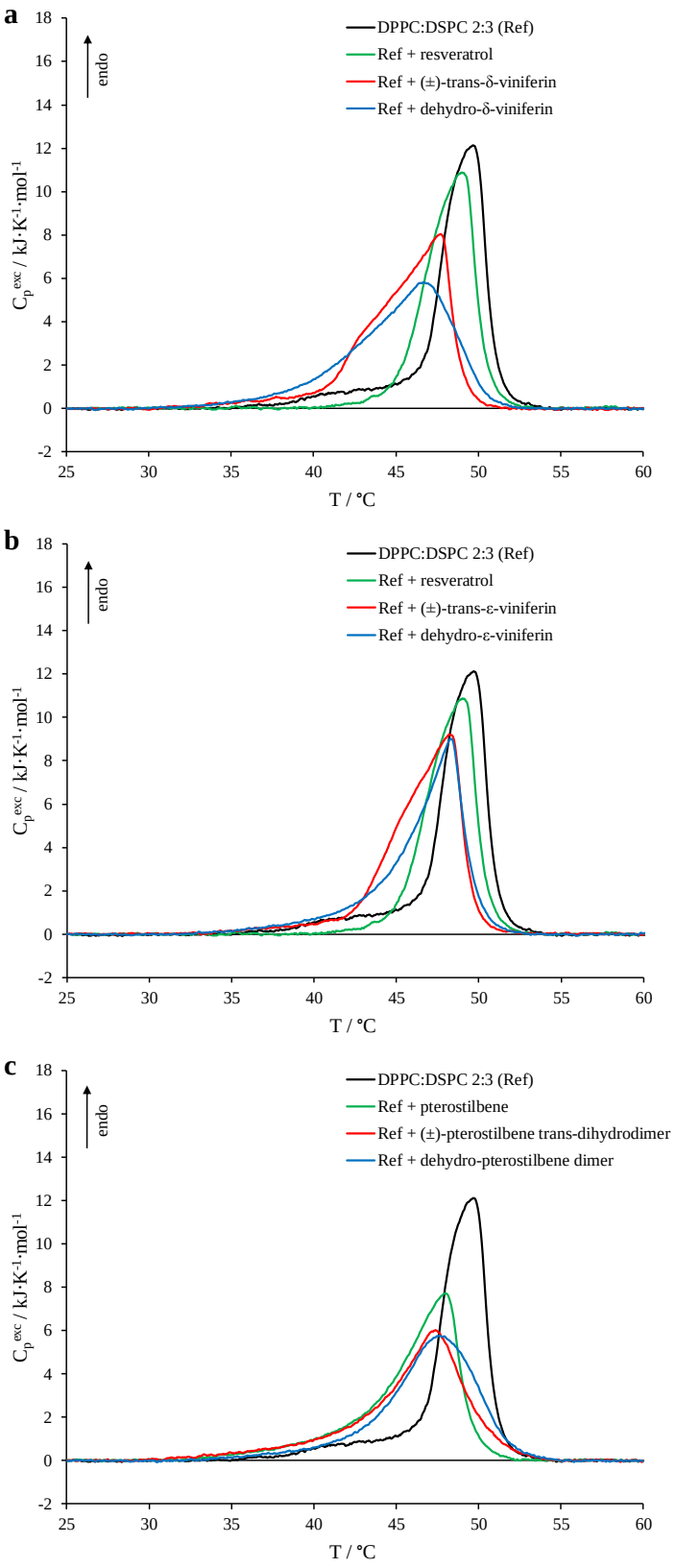

Figure 2. Micro-DSC thermograms for DPPC:DSPC 2:3 vesicles alone (reference black traces) and incorporating the stilbenoid monomers (green traces), dimers (red traces) and dehydro-dimers (blue traces) shown in Figure 1. Specifically, the "monomer / dimer / dehydro-dimer" sets reported are a) resveratrol **1** / (±)-*trans*-δ-viniferin **3** / dehydro-δ-viniferin **6**, b) resveratrol **1** / (±)-*trans*-ε-viniferin **4** / dehydro-ε-viniferin **5** and c) pterostilbene **2** / (±)-pterostilbene *trans*-dihydrodimer **7** / dehydro-pterostilbene dimer **8**. (**1**'s trace is repeated in panel *b* only for showing the complete second set of compounds)

Table 1. Thermodynamic parameters evaluated from micro-DSC investigations for DPPC:DSPC 2:3 vesicles alone (reference system) and incorporating the stilbenoid monomers, dimers and dehydro-dimers shown in Figure 1. The second cycle heating curves were used to obtain the main transition enthalpy ($\Delta H°$), the peak maximum temperature (T_{max}), the transition average temperature ($\overline{T}$) and the average cooperativity index (ACI).

	$\Delta H°$	T_{max}	$\overline{T}$	*ACI*
	kJ·mol^{-1}	**°C**	**°C**	**°C**
DPPC:DSPC 2:3 (Ref)	45 ± 2	49.8 ± 0.1	48.1 ± 0.1	2.8 ± 0.1
Set 1				
Ref + Resveratrol **1**	39 ± 2	49.1 ± 0.2	48.1 ± 0.1	1.7 ± 0.1
Ref + (±)-*trans*-δ-viniferin **3**	41 ± 3	47.6 ± 0.3	45.3 ± 0.3	2.8 ± 0.4
Ref + Dehydro-δ-viniferin **6**	41 ± 2	47.1 ± 0.5	45.1 ± 0.3	3.4 ± 0.1
Set 2				
Ref + Resveratrol **1**	39 ± 2	49.1 ± 0.2	48.1 ± 0.1	1.7 ± 0.1
Ref + (±)-*trans*-ε-viniferin **4**	44 ± 2	48.3 ± 0.1	46.4 ± 0.2	2.7 ± 0.1
Ref + Dehydro-ε-viniferin **5**	41 ± 2	48.3 ± 0.1	46.3 ± 0.1	3.2 ± 0.2
Set 3				
Ref + Pterostilbene **2**	39 ± 2	48.0 ± 0.1	45.7 ± 0.1	3.2 ± 0.1
Ref + (±)-pterostilbene *trans*-dihydrodimer **7**	38 ± 2	47.4 ± 0.1	45.8 ± 0.3	3.7 ± 0.3
Ref + Dehydro-pterostilbene dimer **8**	39 ± 2	47.8 ± 0.1	46.6 ± 0.1	3.3 ± 0.1

The micro-DSC thermograms obtained for the DPPC:DSPC 2:3 reference vesicles and for those incorporating the stilbenoid monomers, dimers and dehydro-dimers shown in Figure 1 (10:1 lipid:stilbenoid molar ratio) are reported in Figure 2, whereas the relevant thermodynamic parameters are listed in Table 1. Further direct comparisons of monomers and dimers effects were also reported in separate figures in Supplementary Material for a better visibility.

All peaks shown in Figure 2 reflect the well-known Ising-like gel-to-liquid crystal transition, *i.e.*, the membrane phase transition from the gel phase, where the phospholipids exhibit the highest order level and tail-tail interaction, to the liquid crystalline phase, in which the phospholipid acyl chains acquire higher mobility leading to a partial loosening of tail-tail van del Waals interactions and level of order. The resulting enthalpy variation ($\Delta H°$) corresponds to the area beneath the calorimetric peak.

The gel-to-liquid crystalline phase transition undergone by the DPPC:DSPC 2:3 reference system provides a broad calorimetric peak (black traces in Figure 2) placed within the temperature range defined by the T_{max} values of the single DPPC's and DSPC's transitions (about 41.6 °C and 54.9 °C,

respectively[26], as typically occurs for multicomponent systems. Specifically, such a profile's width is compatible with systems whose constituents present only partial thermodynamic compatibility, giving rise to a polydisperse distribution of the microstates transition equilibrium constants that presents distinguishable stability clusters or, in other words, a thermodynamic phase separation which is detectable as peak asymmetries and/or shoulders on the calorimetric signal[26,38,39]. Indeed, the profile presents a slight shoulder (at about 48-49 °C) towards the transition temperature corresponding to the phospholipid with the shortest tails (DPPC, the lower-T_m phospholipid), indicating the formation of phases characterized by different lipid molar ratios, as further highlighted by the small step at the beginning of the peak due to the presence of DPPC-rich phases. In any case, we observe that the entropic contributions deriving from the phospholipid constituents follow their proportions, as expected, resulting in a positioning of the calorimetric trace closer to the DSPC T_{max} value. Such an additivity of the contributions is also reflected on the transition enthalpy variation, $\Delta H°$ (Table 1)[26].

As far as the interaction with vesicles is concerned, we observed an increasing destabilizing effect moving from monomers to dimers and to dehydro-dimers (Figure 2). As shown in Table 1, all the destabilizing effects involve both entropic (lowering of the transition average temperature, $\bar{T}$, and reduction of the transition cooperativity, ACI) and enthalpic (lowering of the transition enthalpy, $\Delta H°$) modifications with respect to the reference, being the last ones a clear indication of the interposition of the molecules between the phospholipid tails, which are responsible for the enthalpy variation $\Delta H°$ upon the gel-to-liquid crystal transition through the loosening of van der Waals interactions. On the other hand, the difference in enthalpic contribution among compounds is very small, indicating that their peculiar behaviour is mainly due to entropic contributions, pointing out their role as order-disorder agents.

Going into more details, as regards the first set (Figure 2a, compounds **1**-**3**-**6**), the presence of resveratrol **1** within the bilayer (green trace) leads to the loss of the initial step related to the less stable lipid phases and to an overall downshift of the gel-to-liquid crystal transition interval. A further destabilization is progressively observed when moving from **3** to **6** (red and blue traces, respectively) in terms of loss of transition cooperativity (increasing ACI values in Table 1) and downshift of the $\bar{T}$. Indeed, larger and shouldered peaks are produced and reflect an enhancement of a phase separation favouring the formation of DPPC-rich phases. The severe difference between the DSC profiles of dimer **3** and dehydro-dimer **6** might be merely ascribable to different geometrical features and exclusion volumes, that influence the polydispersity of the phospholipid phase stability distribution and the phase separation[31]. Indeed, (±)-*trans*-δ-viniferin **3** is characterized by a three-dimensional structure that likely encumbers the lipid packing and seems to promote phospholipid packing

reorganization leading to the formation of visible DPPC-rich lipid phases (low-temperature shoulder on red profile, Figure 2a)[25]. Instead, the geometry of **6** allows a more homogeneous lipid phase distribution reflected in the absence of evident shoulders in the DSC profile even though presenting a broadening towards the least stable phases.

To sum up, all the compounds of the first set are well incorporated into the membrane and the magnitude of the destabilizing effects follows the order **1** < **3** < **6**.

The same general trend observed was also maintained for the second set, which includes the ε-dimers (**1** < **4** < **5**, Figure 2b). However, we observed that ε-dimer **4** and ε-dehydrodimer **5** cause less thermodynamic destabilization of the membrane than the respective δ-homologues **3** and **6**, which may be ascribable to their compact geometry and hence a less perturbation bilayer's lipid packing.

The picture emerged from the last set, *i.e.*, the compounds with the presence of the -OMe substitution (Figure 2c, compounds **2**-**7**-**8**), indicates that pterostilbene **2** produces a severe entropic and enthalpic destabilization of the membrane already as a monomer, as also indicated by the parameters in Table 1. Such a different behaviour with respect to resveratrol **1** may be ascribed to its higher lipophilicity, which allows **2** to reside better within the membrane hydrophobic core. On the other hand, dimer **7** and dehydro-dimer **8** produce both similar effects, *i.e.*, a slight further entropic destabilization of the membrane with respect to **2** (**2** < **7** ≈ **8**) (Table 1).

We may highlight here that, during the aforementioned experiments, we directly mixed phospholipids and the selected stilbenoid prior to dissolve them in the organic solvent for the preparation of the liposomal dispersions, in order to assess their effects at the maximum incorporation level. Nevertheless, considering that in real antimicrobial assays the first stilbenoid-bilayer interaction occurs on the outer surface of the microbial membrane, for the sake of completeness we performed additional measurements aimed at highlighting peculiarities on the inclusion process of the compounds from the external environment. For this purpose, we added selected compounds to the preformed model 2:3 DPPC:DSPC vesicles up to the same lipid:stilbenoid ratio considered above (see Materials and Methods section). Specifically, compounds **6**, **7** and **8**, which exhibited major effects on the membrane stability when already incorporated, were selected to investigate the effects of both the geometry and substitution pattern on the inclusion process from the external environment.

The micro-DSC thermograms obtained for DPPC:DSPC 2:3 vesicles with the external addition of dehydro-δ-viniferin **6**, (±)-pterostilbene *trans*-dihydrodimer **7** and dehydro-pterostilbene dimer **8** from DMSO solutions are reported in Figure 3. For these measurements, the first heating scans were compared since they may be considered as the first shot of the stilbenoid-membrane interaction.

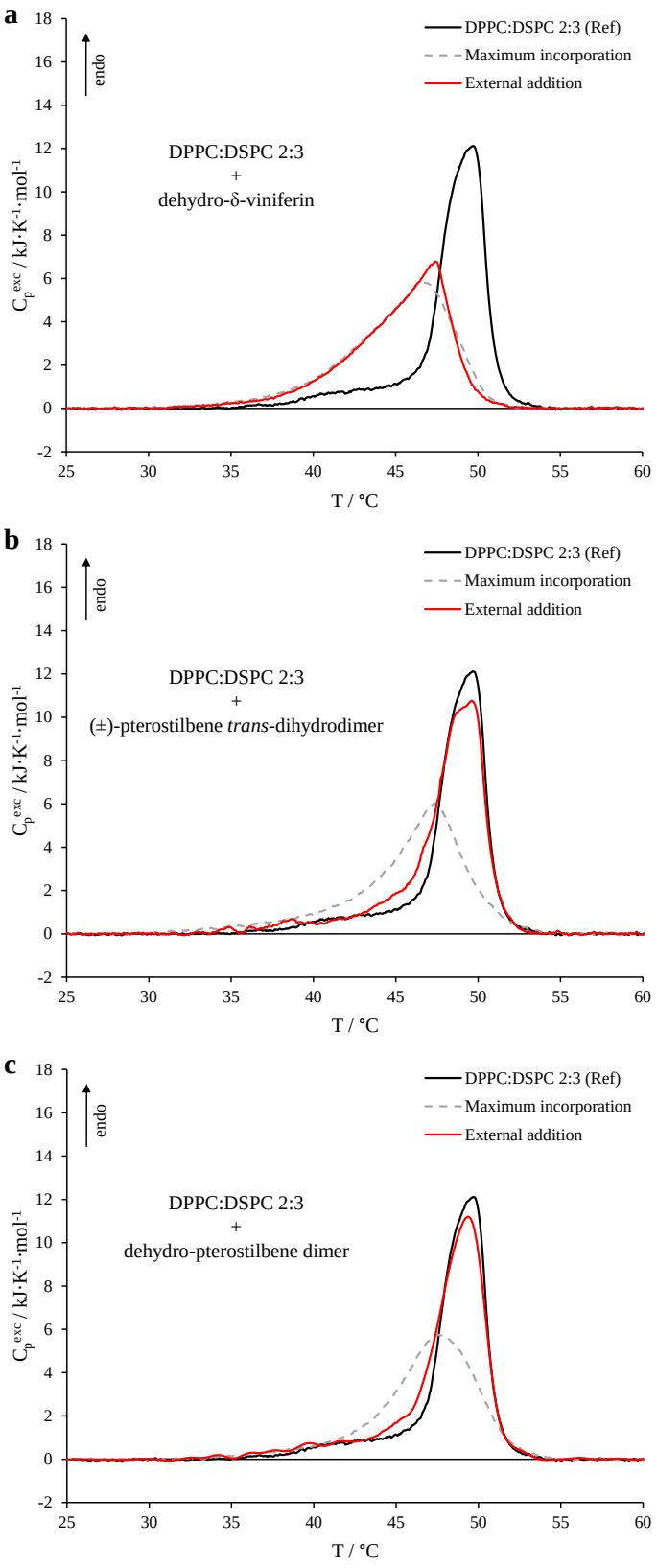

Figure 3. Micro-DSC thermograms (first heating scans) obtained for DPPC:DSPC 2:3 vesicles with the external addition of a) dehydro-δ-viniferin **6**, b) (±)-pterostilbene *trans*-dehydrodimer **7** and c) dehydro-pterostilbene dimer **8** from DMSO solutions (red curves). The profiles obtained for DPPC:DSPC 2:3 vesicles and for those with the maximum incorporation of the respective stilbenoids are also reported from Figure 2 for the sake of comparison (black solid curve and grey dashed one, respectively).

The external addition of **6** to the model membrane immediately results in similar effects to those achieved by the direct mixing of the compound with phospholipids (Figure 3a). Indeed, the DSC profile (red trace) is superimposable to the one obtained with the maximum incorporation discussed above (reported as a grey dashed trace for the sake of comparison), and the same enthalpy was observed upon the gel-to-liquid crystal transition ($\Delta H° = 40 \pm 2$ kJ·mol^{-1}), confirming the ability of **6** to go beyond the hydrophilic surface of the membrane and to full incorporate into the hydrophobic core. On the other hand, the external addition of **8**, which has the same planar structure as **6** and only differs for the -OMe substitution, leads to no significant effects on the thermotropic behaviour of the model membrane (red trace in Figure 3c), revealing the poor insertion of the compound into the bilayer. The same behaviour was observed for compound **7**, characterized by a different geometry but the same substitution pattern as **8**, as clearly visible in Figure 3b.

This evidence suggests that the -OH substitution plays a crucial role on the insertion mechanism. Indeed, the five hydroxyl groups of **6** may easily interact with the phospholipid headgroups by means of hydrogen bonds. Such interactions might drive the approach of the compound to the vesicle outer leaflet and then the insertion of the whole structure into the bilayer for hydrophobic effect. On the other hand, when four out of five hydroxyl groups are methylated to get **7** and **8**, the residual –OH group is no longer sufficient to anchor the molecules at the vesicle surface, resulting in a poor insertion of the compounds into the liposome hydrophobic core.

Nevertheless, we should consider here that the addition of the compounds was performed at room temperature, *i.e.*, at a temperature in which the model membrane is in the "gel" phase. Instead, real cell membranes at physiological conditions may present regions that are already in the "liquid crystalline" phase, whose properties might allow an easier insertion of the compounds. For this reason, in order to provide the compounds with a membrane in the liquid crystalline phase, as well as to ensure the absence of metastable lipid phases, further heating/cooling cycles were performed. Although the resulting thermograms show a slight enhancement of the interaction between **7**-**8** and the membrane, the kind and the magnitude of such interaction do not modify the overall picture emerging from Figure 3 (see Supplementary Material).

Although the simplicity of the model membrane used and being aware that the microbiological systems are very complex and other pathways by which stilbenoids may explicate their antimicrobial activity cannot be excluded, the overall picture emerged by means of the micro-DSC technique as concerns the magnitude of the stilbenoid-membrane destabilizing interaction well correlates with the reported microbiological activity data[22].

As regards the first set of compounds (Figure 2a), the enhancement of the destabilizing interactions (**1** < **3** < **6**) observed by DSC perfectly matches the trend of the previously reported

minimum inhibitory concentration (MIC) and minimum bactericidal concentration (MBC) activity with **6** as the most active compound[22]. Analogously, the picture exhibited by the second set (**1** < **4** < **5**, Figure 2b) reflects the microbiological data trend as well. Since the above-mentioned compounds do not present -OMe groups, we may conclude that they are able to insert into the membrane and to exhibit different membrane destabilizing actions following the pattern revealed by Figure 2, according to their structure.

By contrast, in the case of the third set, which is characterized by -OMe substitutions, the correlation between the interaction order emerged from the DSC analysis (**2** < **7** ≈ **8**, Figure 2c) obtained for the systems which already included the compounds into the membrane hydrophobic core and the microbiological data is missing, but, on the other hand are coherent with the external insertion data highlighting the crucial role of -OH groups the insertion step (Figure 3).

NMR spectroscopy

Complementary information about the stilbenoid-membrane interaction were achieved through NMR Nuclear Overhauser effect spectroscopy (NOESY), which is based on the transfer of nuclear spin polarization from one nuclear spin population to another spin via dipole-dipole cross-relaxation. NOESY is a powerful tool for studying intermolecular complexes. However, its application to molecules-cell membranes interaction studies may be difficult, because relaxation times for phospholipid aggregates are too large compared with the NMR chemical shift time scale.[40–44] Therefore, the hydrophobic environment of a bacterial membrane was simulated by sodium dodecylsulfate (SDS), one of the most widely used surfactants for the membrane modeling in NMR field.[45–50] Indeed, the SDS micelles have a larger correlation time with respect to the NMR time-scale and their small size allows a good spectral resolution.[40] Furthermore, the SDS polar headgroup (the sulphate moiety) mimics the membranes surface and many important phenomena which take place in bilayer membranes can be elucidated by experiments on the monolayer at an interface.[37,51]

NMR experiments were conducted on water soluble derivatives, namely resveratrol **1** as monomeric compound and the two dimers (±)-*trans*-ε-viniferin **4** and dehydro-δ-viniferin **6**, the least active and most active antimicrobial compounds, respectively.[22]

Initially, we focused of the parent compound resveratrol **1**, whose interactions with model membranes have already been studied by other groups.[52,53] The resveratrol protons' signals appear sharp and well separated and they are easily assigned: four signals in the range of 7.6-6.9 ppm are assigned to the olefinic (α,α') and aromatic protons (H2',6' and H3',5') of *para*-substituted ring (A),

whilst only one aromatic proton of the *para*-substituted ring (B) (H4) is observed in our conditions because of the exchange mechanism that involves the H 2,6 aromatic protons with D_2O (Table S1).

The contacts of the ligand with the SDS micelles can occur: (*i*) at the level of methylene group close to the SDS' hydrophilic head (CH_2-12, signals at 4.11 ppm in the ^1H NMR spectrum) and of the neighboring methylene group (CH_2-11, signal at 1.72 ppm); (*ii*) at the level of the terminal methyl group (CH_3-1, signal at 0.90 ppm) and/or the nine remaining methylenes (signal at 1.31 ppm) in the inner hydrophobic core of the micelle.

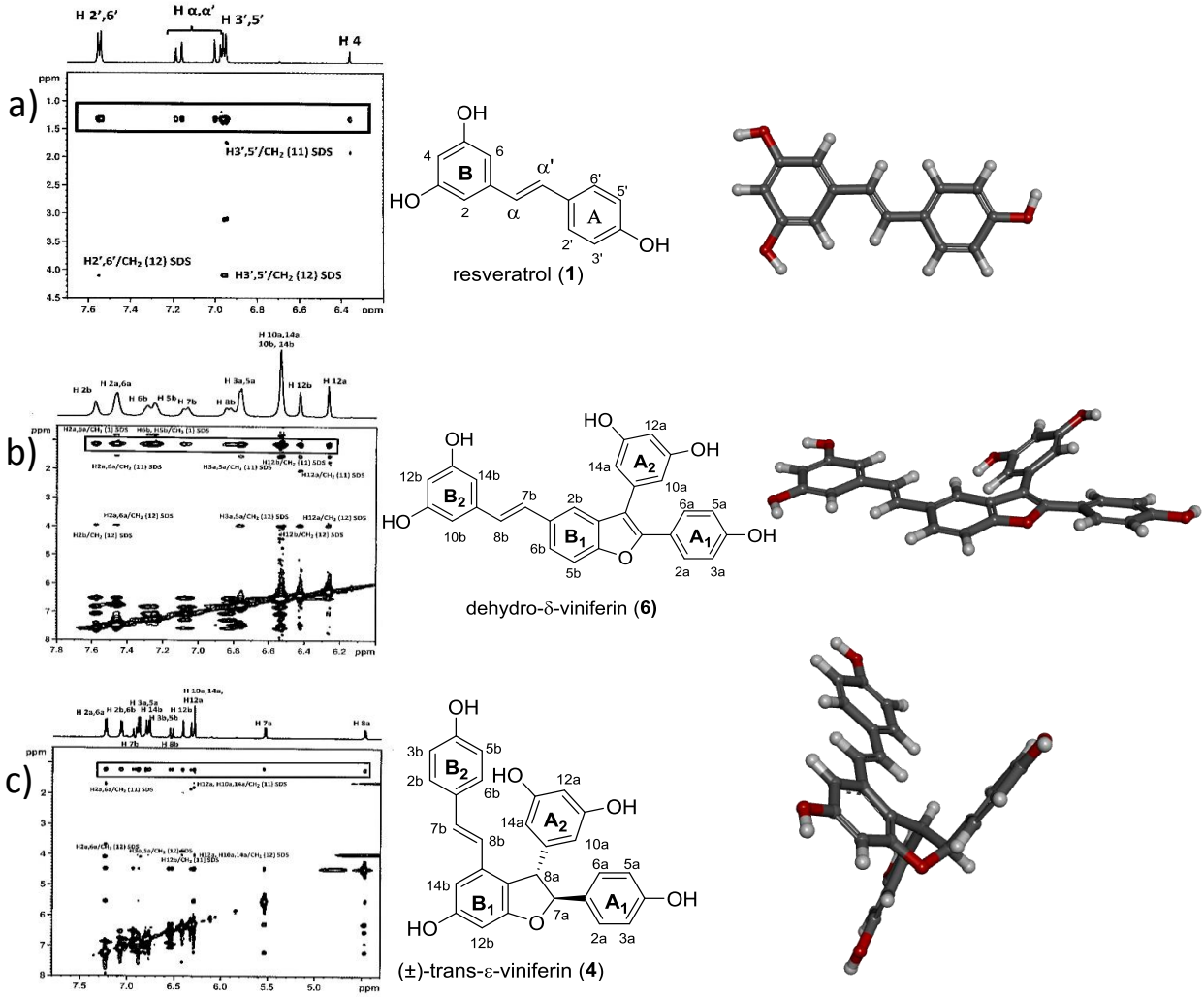

Figure 4. Selected region of 2D ROESY spectra with SDS micelles and models of spatial structures of (a) **1**; (b) **6** and (c) **4**. The boxes in 2D spectra display the intermolecular NOE interactions between lipophilic chain of SDS with all protons of **1**, **6** and **4**.

To evaluate the interactions of resveratrol with SDS micelles we performed ROESY experiments, *i.e.*, NOE experiments in a rotating frame. It is worth noting that ROESY experiments were chosen

to avoid spin diffusion (indirect magnetization transfer) that can occur at long mixing times. NOE/ROE cross peaks between two protons allows to deduce that the protons are close within a distance of 5 Å.

2D ROESY experiments showed that all resveratrol protons, including olefinic α and α', have contacts with the methylene groups of the lipophilic chain of SDS. Interestingly, no NOEs interactions are detected between resveratrol protons and CH_3 (1) of the tail of SDS.

H2',6' and H3',5' aromatic protons on ring A interact with methylene protons 11 and 12 of the polar head of SDS (Figure 4a). Overall, these findings indicate that resveratrol is inserted with ring B close to the lipophilic chain whereas ring A is near to the polar head of the SDS, assuming a "parallel" position with respect to the mimetic membrane (Table 2).

Successively, the interactions of compounds **6** and **4** were investigated. The dehydro-δ-viniferin **6** signals appear quite broad in the ^{1}H NMR spectrum. 2D COSY experiment allowed to assign the H7 and H8 olefinic protons at 7.09 and 6.84 ppm and all the aromatic protons (Table S1 and Figure S6).

2D ROESY experiments allowed to detect a certain number of intra- and intermolecular NOE contacts: a) all dehydro-δ-viniferin's protons, including olefinic H7 and H8, show contacts with methylene groups of the lipophilic chain of SDS; b) aromatic protons of ring A1 show NOE contacts with CH_2 (12) and CH_2(11) of the polar head of SDS. The aromatic protons H10a,14a and H10b,14b show interactions with the polar head of SDS as well, but it was not possible to unambiguously assign them because of their overlapping. Additionally, a small NOE contact of H2b of ring B1 was detected with the polar head group of the SDS; c) aromatic protons H5b and H6b show NOE contacts with methyl group of the lipophilic chain of SDS. No NOE were observed between olefinic H7 and H8 protons with the methyl group of SDS. Beside these NOEs contacts, interactions between H12b/CH_2 (12), CH_2 (11) and H2,6a/methyl group were observed (Table 2 and Figure 4b). Overall, these findings indicate that the dehydro-δ-viniferin is inserted with the rings B2 into the micelles while the rings A1 and A2 are positioned close to the polar head of the SDS in an "inclined" orientation respect to the SDS chain.

Table 2. Intermolecular NOEs observed between SDS and resveratrol **1**, dehydro-δ-viniferin **6** and (±)-*trans*-ε-viniferin **4**.

SDS protons	**1**	**6**	**4**
CH_2(12)	H3',5'	H3a,5a	H3a,5a
CH_2(12)	H2',6'	H2a,6a	H2a,6a
CH_2 (12)		H12a	
CH_2(12)	-	H2b	
CH_2(12)	-	H12b	H12b
CH_2(11)	H3',5'	H3a,5a	H3a,5a
CH_2(11)	H2',6'	H2a,6a	H2a,6a
CH_2(11)		H12a	
CH_2(11)	-	H12b	H12b
CH_2(chain)	All protons	All protons	All protons
CH_3 (1)	Zero NOEs	H5b	
CH_3(1)	-	H6b	
CH_3(1)	-	H2a,6a	

The (±)-*trans*-ε-viniferin **4** protons appear sharp in SDS micelles (Table S1 and Figure S7). All the (±)-*trans*-ε-viniferin protons show contacts with the methylene groups of the lipophilic chain of SDS and a weak NOE was detected between aromatic protons of A1 ring and H12b with methylene 11 and 12 of SDS. No NOEs interactions were found between (±)-*trans*-ε-viniferin **4** protons and CH_3 (1) of the tail of SDS (Table 2 and Figure 4c). From our results it emerges that **4** inserts into the SDS micelles with the A1 and A2 rings near the polar head of SDS but with a different orientation respect to the dehydro-δ-viniferin. However, whereas the most favorable location for **6** in SDS micelles is within the core, for **1** and **4** the best location is closer to the head groups.

NMR findings are in agreement and well complement those obtained by DSC studies. Overall, our results suggest that the shape, stereochemistry and substitution pattern of stilbenoid scaffold play a crucial role for the interaction with the membrane.

The overall data suggest that the effects of stilbenoids on the membrane bilayer may be ascribed to the penetration of the compounds into the phospholipid bilayer. In our hypothesis, stilbenoids approach the bilayer membrane by forming strong hydrogen bonds between their -OH groups and oxygen atoms of the lipid headgroups and then penetrate the bilayer through hydrophobic interactions with the lipid tail region. Our hypothesis is in agreement with molecular dynamics study on the

biophysical interactions of catechins with POPC (1-palmitoyl-2-oleoylphosphatidylcholine) lipid bilayer model of cell membranes.[54]

The different location in the SDS micelles of **1**, **4** and **6** can be explained by their conformational structure. Resveratrol **1**, which possesses a completely planar structure (Figure 4a), is able to enter and accommodate into the lipid layer, with a moderate disturbing effect on the membrane assembly. Compound **6** can penetrate into the hydrophobic region of fatty acyl chains of the membrane as well, due to the high degree of hydrophobicity of the aromatic hydrocarbon and hydrogen bonding of the phenolic hydroxyl groups, as well as to the planarity of the aromatic system. However, the orientation of ring A2, which is not coplanar with the system A1-B1-B2, forces a rearrangement of the lipid packing (Figure 4b). This evidence is in line with the micro-DSC data and the effect may compromise the cell membrane functionality and eventually lead to the death of the bacteria. Conversely, despite the shape of compound **4** (Figure 4c) allows the penetration of the molecule into the lipophilic layer, it creates a weaker disturbing effect on the membrane, which is in line with the very low antimicrobial activity of the compound.

Conclusions

The data presented in this work allowed to confirm the direct stilbenoid-membrane interaction, discriminating among the thermodynamic and structural determinants that drive the resveratrol-derived monomers and dimers influence on the membrane stability. In particular, three complete "monomer / dimer / dehydro-dimer" sets were investigated by evaluating the effects deriving from the maximum stilbenoid-membrane interaction, as well as the peculiarities of the process of stilbenoids incorporation into the hydrophobic portion of phospholipid bilayer.

The experimental data indicate that the stilbenoids interaction with the membrane is strongly influenced by the structure of the compound, both in terms of geometry and substitution pattern. Specifically, the increase of steric hindrance and lipophilicity occurring when moving from monomers (**1** and **2**) to dimers (**3**, **4** and **7**) induces a severe phase separation that displays a favourable interaction of the compounds with the DPPC (the phospholipid with the shortest tail and the lowest T_m), and whose magnitude strictly depends on the substitution pattern (**3** vs **7**) and the isomerism (**3** vs **4**). On the other hand, the stilbenoid-membrane interaction is further enhanced when moving to dehydro-dimers (**5**, **6** and **8**). Indeed, the inclusion of planar structures between the phospholipid tails leads to an increased entropic membrane destabilization.

Nevertheless, the involvement of the cell membrane in the antimicrobial action of such stilbenoids against food pathogens does not overlook the process of inclusion of the compounds into the membrane's hydrophobic core, being negatively affected in some cases. Indeed, our experiments

show how an adequate hydrophilicity is needed to gain a successful approach of the compounds to the membrane's outer polar headgroups by establishing hydrogen bonds and hence drive the compound into the membrane (**6** vs **7**-**8**).

We would like to emphasize here again that the microbiological systems are very complex and other pathways by which stilbenoids may explicate their antimicrobial activity cannot be excluded. However, being aware of this possibility, the overall picture emerged from this work as concerns the magnitude of the stilbenoid-membrane destabilizing interaction well correlates with the microbiological activity data previously reported in the literature.[22]

In order to have a clear picture of the interaction of stilbenoids with a model membrane, all the experiments were performed using single pure compounds. However, it should be stressed that, in a real setting, stilbenoid extracts contain complex phenolic profiles and their action on cell membranes would be difficult to predict *ab initio* due to potential synergistic or competitive effects. In a future prospective, efforts will be directed on the investigation of crude and enriched extracts following the results emerged from this study.

To conclude, the present study offers insights into the forces that drive the interaction of stilbenoids with cell membranes and may help to identify bioactive health-promoting compounds in the frame of healthcare, human food and animal feeds.

Author contributions

Conceptualization – SD, AP and DF; Data curation – SM and MS; Formal analysis – FS, SM, DF; Investigation – FS, SM and LM; Methodology – FS, SM and DF; Resources – SD, AP and DF; Supervision – AP and DF; Writing – original draft – FS and SM; Writing - review & editing – all authors. All authors have read and agreed to the published version of the manuscript.

Conflicts of interest

There are no conflicts of interest to declare.

Acknowledgments

The research was partly supported by "Transition Grant 2015-2017 - Linea 1A" of the University of Milan.

References

1 M. D. Kirk, S. M. Pires, R. E. Black, M. Caipo, J. A. Crump, B. Devleesschauwer, D. Döpfer, A. Fazil, C. L. Fischer-Walker, T. Hald, A. J. Hall, K. H. Keddy, R. J. Lake, C. F.

Lanata, P. R. Torgerson, A. H. Havelaar and F. J. Angulo, World Health Organization Estimates of the Global and Regional Disease Burden of 22 Foodborne Bacterial, Protozoal, and Viral Diseases, 2010: A Data Synthesis, *PLoS Med.*, 2015, **12**, 1–21.

2 D. S. L. Ma, L. T. H. Tan, K. G. Chan, W. H. Yap, P. Pusparajah, L. H. Chuah, L. C. Ming, T. M. Khan, L. H. Lee and B. H. Goh, Resveratrol-potential antibacterial agent against foodborne pathogens, *Front. Pharmacol.*, 2018, **9**, 1–16.

3 M. Riva, D. Fessas and A. Schiraldi, Isothermal calorimetry approach to evaluate shelf life of foods, *Thermochim. Acta*, 2001, **370**, 73–81.

4 M. Takó, E. B. Kerekes, C. Zambrano, A. Kotogán, T. Papp, J. Krisch and C. Vágvölgyi, Plant phenolics and phenolic-enriched extracts as antimicrobial agents against food-contaminating microorganisms, *Antioxidants*, , DOI:10.3390/antiox9020165.

5 L. Bouarab Chibane, P. Degraeve, H. Ferhout, J. Bouajila and N. Oulahal, Plant antimicrobial polyphenols as potential natural food preservatives, *J. Sci. Food Agric.*, 2019, **99**, 1457–1474.

6 B. C. Akinwumi, K. A. M. Bordun and H. D. Anderson, Biological activities of stilbenoids, *Int. J. Mol. Sci.*, 2018, **19**, 1–25.

7 D. B. Niesen, C. Hessler and N. P. Seeram, Beyond resveratrol: A review of natural stilbenoids identified from 2009-2013, *J. Berry Res.*, 2013, **3**, 181–196.

8 R. Casadey, C. Challier, M. Altamirano, M. B. Spesia and S. Criado, Antioxidant and antimicrobial properties of tyrosol and derivative-compounds in the presence of vitamin B2. Assays of synergistic antioxidant effect with commercial food additives, *Food Chem.*, 2021, **335**, 127576.

9 D. Del Rio, A. Rodriguez-Mateos, J. P. E. Spencer, M. Tognolini, G. Borges and A. Crozier, Dietary (poly)phenolics in human health: Structures, bioavailability, and evidence of protective effects against chronic diseases, *Antioxidants Redox Signal.*, 2013, **18**, 1818–1892.

10 V. Sáez, E. Pastene, C. Vergara, C. Mardones, I. Hermosín-Gutiérrez, S. Gómez-Alonso, M. V. Gómez, C. Theoduloz, S. Riquelme and D. von Baer, Oligostilbenoids in Vitis vinifera L. Pinot Noir grape cane extract: Isolation, characterization, in vitro antioxidant capacity and anti-proliferative effect on cancer cells, *Food Chem.*, 2018, **265**, 101–110.

11 C. Rivière, A. D. Pawlus and J. M. Mérillon, Natural stilbenoids: Distribution in the plant kingdom and chemotaxonomic interest in Vitaceae, *Nat. Prod. Rep.*, 2012, **29**, 1317–1333.

12 R. F. Guerrero, B. Biais, T. Richard, B. Puertas, P. Waffo-Teguo, J. M. Merillon and E. Cantos-Villar, Grapevine cane's waste is a source of bioactive stilbenes, *Ind. Crops Prod.*, 2016, **94**, 884–892.

13 M. J. Aliaño-González, T. Richard and E. Cantos-Villar, Grapevine Cane Extracts: Raw Plant Material, Extraction Methods, Quantification, and Applications, *Biomol. 2020, Vol. 10, Page 1195*, 2020, **10**, 1195.

14 H. Soto-Valdez, R. Auras and E. Peralta, Fabrication of poly(lactic acid) films with resveratrol and the diffusion of resveratrol into ethanol, *J. Appl. Polym. Sci.*, 2011, **121**, 970–978.

15 S. Cruz, R. Raposo, M. J. Ruiz-Moreno, T. Garde-Cerdán, B. Puertas, A. Gonzalo-Diago, J. M. Moreno-Rojas and E. Cantos-Villar, Grapevine-shoot stilbene extract as a preservative in white wine, *Food Packag. Shelf Life*, 2018, **18**, 164–172.

16 M. C. Santos, C. Nunes, J. A. Saraiva and M. A. Coimbra, Chemical and physical methodologies for the replacement/reduction of sulfur dioxide use during winemaking: Review of their potentialities and limitations, *Eur. Food Res. Technol.*, 2012, **234**, 1–12.

17 A. García-Ruiz, B. Bartolomé, A. J. Martínez-Rodríguez, E. Pueyo, P. J. Martín-Álvarez and M. V. Moreno-Arribas, Potential of phenolic compounds for controlling lactic acid bacteria growth in wine, *Food Control*, 2008, **19**, 835–841.

18 E. P. Díaz-Galindo, A. Nesic, G. Cabrera-Barjas, O. Dublan-García, R. I. Ventura-Aguilar, F. J. Vázquez-Armenta, S. A.-M. de Oca, C. Mardones and J. F. Ayala-Zavala, Physico-Chemical and Antiadhesive Properties of Poly(Lactic Acid)/Grapevine Cane Extract Films against Food Pathogenic Microorganisms, *Polym. 2020, Vol. 12, Page 2967*, 2020, **12**, 2967.

19 M. D. Martinotti, S. J. Castellanos, R. González, A. Camargo and M. Fanzone, Nematicidal effects of extracts of garlic, grape pomace and olive mill waste, on Meloidogyne incognita, on grapevine cv Chardonnay., *Rev. la Fac. Ciencias Agrar. Univ. Nac. Cuyo*, 2016, **48**, 211–224.

20 R. Gutiérrez-Escobar, M. I. Fernández-Marín, T. Richard, A. Fernández-Morales, M. Carbú, C. Cebrian-Tarancón, M. J. Torija, B. Puertas and E. Cantos-Villar, Development and characterization of a pure stilbene extract from grapevine shoots for use as a preservative in wine, *Food Control*, 2021, **121**, 107684.

21 S. Rayne, E. Karacabey and G. Mazza, Grape cane waste as a source of trans-resveratrol and

606 trans-viniferin: High-value phytochemicals with medicinal and anti-phytopathogenic
607 applications, *Ind. Crops Prod.*, 2008, **27**, 335–340.

608 22 L. M. Mattio, S. Dallavalle, L. Musso, R. Filardi, L. Franzetti, L. Pellegrino, P. D'Incecco,
609 D. Mora, A. Pinto and S. Arioli, Antimicrobial activity of resveratrol-derived monomers and
610 dimers against foodborne pathogens, *Sci. Rep.*, 2019, **9**, 19525.

611 23 Y. Wu, J. Bai, K. Zhong, Y. Huang, H. Qi, Y. Jiang and H. Gao, Antibacterial activity and
612 membrane-disruptive mechanism of 3-p-trans-coumaroyl-2-hydroxyquinic acid, a novel
613 phenolic compound from pine needles of Cedrus deodara, against Staphylococcus aureus,
614 *Molecules*, 2016, **21**, 1084.

615 24 F. Saitta, M. Signorelli and D. Fessas, Hierarchy of interactions dictating the
616 thermodynamics of real cell membranes: Following the insulin secretory granules paradigm
617 up to fifteen-components vesicles, *Colloids Surfaces B Biointerfaces*, 2020, **186**, 110715.

618 25 F. Saitta, P. Motta, A. Barbiroli, M. Signorelli, C. La Rosa, A. Janaszewska, B. Klajnert-
619 Maculewicz and D. Fessas, Influence of Free Fatty Acids on Lipid Membrane-Nisin
620 Interaction, *Langmuir*, 2020, **36**, 13535–13544.

621 26 F. Saitta, M. Signorelli and D. Fessas, Dissecting the effects of free fatty acids on the
622 thermodynamic stability of complex model membranes mimicking insulin secretory granules,
623 *Colloids Surfaces B Biointerfaces*, 2019, **176**, 167–175.

624 27 K. N. Kontogiannopoulos, A. Dasargyri, M. F. Ottaviani, M. Cangiotti, D. Fessas, V. P.
625 Papageorgiou and A. N. Assimopoulou, Advanced Drug Delivery Nanosystems for Shikonin:
626 A Calorimetric and Electron Paramagnetic Resonance Study, *Langmuir*, 2018, **34**, 9424–
627 9434.

628 28 N. Naziris, F. Saitta, V. Chrysostomou, M. Libera, B. Trzebicka, D. Fessas, S. Pispas and C.
629 Demetzos, pH-responsive chimeric liposomes: From nanotechnology to biological
630 assessment, *Int. J. Pharm.*, 2020, **574**, 118849.

631 29 A. Laouini, C. Jaafar-Maalej, I. Limayem-Blouza, S. Sfar, C. Charcosset and H. Fessi,
632 Preparation, Characterization and Applications of Liposomes: State of the Art, *J. Colloid Sci.*
633 *Biotechnol.*, 2012, **1**, 147–168.

634 30 R. C. MacDonald, R. I. MacDonald, B. P. M. Menco, K. Takeshita, N. K. Subbarao and L.
635 rong Hu, Small-volume extrusion apparatus for preparation of large, unilamellar vesicles,
636 *BBA - Biomembr.*, 1991, **1061**, 297–303.

31 K. Gardikis, S. Hatziantoniou, M. Signorelli, M. Pusceddu, M. Micha-Screttas, A. Schiraldi, C. Demetzos and D. Fessas, Thermodynamic and structural characterization of Liposomal-Locked in-Dendrimers as drug carriers, *Colloids Surfaces B Biointerfaces*, 2010, **81**, 11–19.

32 S. Bonora, S. A. Markarian, A. Trinchero and K. R. Grigorian, DSC study on the effect of dimethysulfoxide (DMSO) and diethylsulfoxide (DESO) on phospholipid liposomes, *Thermochim. Acta*, 2005, **433**, 19–26.

33 M. Ricci, R. Oliva, P. Del Vecchio, M. Paolantoni, A. Morresi and P. Sassi, DMSO-induced perturbation of thermotropic properties of cholesterol-containing DPPC liposomes, *Biochim. Biophys. Acta - Biomembr.*, 2016, **1858**, 3024–3031.

34 G. Barone, P. Del Vecchio, D. Fessas, C. Giancola and G. Graziano, THESEUS: A new software package for the handling and analysis of thermal denaturation data of biological macromolecules, *J. Therm. Anal.*, 1992, **38**, 2779–2790.

35 A. Barbiroli, F. Bonomi, P. Ferranti, D. Fessas, A. Nasi, P. Rasmussen and S. Iametti, Bound fatty acids modulate the sensitivity of bovine β-lactoglobulin to chemical and physical denaturation, *J. Agric. Food Chem.*, 2011, **59**, 5729–5737.

36 L. F. Galiullina, I. Z. Rakhmatullin, E. A. Klochkova, A. V. Aganov and V. V. Klochkov, Structure of pravastatin and its complex with sodium dodecyl sulfate micelles studied by NMR spectroscopy, *Magn. Reson. Chem.*, 2014, **53**, 110–114.

37 I. Z. Rakhmatullin, L. F. Galiullina, E. A. Klochkova, I. A. Latfullin, A. V. Aganov and V. V. Klochkov, Structural studies of pravastatin and simvastatin and their complexes with SDS micelles by NMR spectroscopy, *J. Mol. Struct.*, 2016, **1105**, 25–29.

38 P. Losada-Pérez, N. Mertens, B. de Medio-Vasconcelos, E. Slenders, J. Leys, M. Peeters, B. van Grinsven, J. Gruber, C. Glorieux, H. Pfeiffer, P. Wagner and J. Thoen, Phase Transitions of Binary Lipid Mixtures: A Combined Study by Adiabatic Scanning Calorimetry and Quartz Crystal Microbalance with Dissipation Monitoring, *Adv. Condens. Matter Phys.*, 2015, **2015**, 1–14.

39 S. Mabrey and J. M. Sturtevant, Investigation of phase transitions of lipids and lipid mixtures by sensitivity differential scanning calorimetry., *Proc. Natl. Acad. Sci.*, 1976, **73**, 3862–3866.

40 G. S. Shurshalova, A. R. Yulmetov, D. A. Sharapova, A. V. Aganov and V. V. Klochkov, Interaction of Lovastatin with Model Membranes by NMR Data and from MD Simulations, *Bionanoscience*, 2020, **10**, 493–501.

41 L. F. Galiullina, O. V. Aganova, I. A. Latfullin, G. S. Musabirova, A. V. Aganov and V. V. Klochkov, NMR Study of Conformational Structure of Fluvastatin and Its Complex with Dodecylphosphocholine Micelles, *Bionanoscience*, 2016, **6**, 352–354.

42 L. F. Galiullina, O. V. Aganova, I. A. Latfullin, G. S. Musabirova, A. V. Aganov and V. V. Klochkov, Interaction of different statins with model membranes by NMR data, *Biochim. Biophys. Acta - Biomembr.*, 2017, **1859**, 295–300.

43 L. F. Galiullina, G. S. Musabirova, I. A. Latfullin, A. V. Aganov and V. V. Klochkov, Spatial structure of atorvastatin and its complex with model membrane in solution studied by NMR and theoretical calculations, *J. Mol. Struct.*, 2018, **1167**, 69–77.

44 I. A. Latfullin, L. F. Galiullina, G. S. Musabirova, O. V. Aganova, Z. F. Kim, A. V. Aganov and V. V. Klochkov, Statins and their interaction with model cell membranes according to the data of nuclear magnetic resonance spectroscopy, *Ration. Pharmacother. Cardiol.*, 2017, **13**, 256–262.

45 D. A. Kaluck, M. R. Tessmer, C. R. Watts and C. Y. Li, The Use of Dodecylphosphocholine Micelles in Solution NMR, *J. Magn. Reson. Ser. B*, 1995, **109**, 60–65.

46 G. Manzo, M. Carboni, A. C. Rinaldi, M. Casu and M. A. Scorciapino, Characterization of sodium dodecylsulphate and dodecylphosphocholine mixed micelles through NMR and dynamic light scattering, *Magn. Reson. Chem.*, 2013, **51**, 176–183.

47 L. Mäler and A. Gräslund, Artificial membrane models for the study of macromolecular delivery, *Methods Mol. Biol.*, 2009, **480**, 129–139.

48 E. Sikorska, D. Wyrzykowski, K. Szutkowski, K. Greber, E. A. Lubecka and I. Zhukov, Thermodynamics, size, and dynamics of zwitterionic dodecylphosphocholine and anionic sodium dodecyl sulfate mixed micelles, *J. Therm. Anal. Calorim.*, 2016, **123**, 511–523.

49 A. M. Seddon, P. Curnow and P. J. Booth, *Biochim. Biophys. Acta - Biomembr.*, 2004, 1666, 105–117.

50 K. S. Usachev, S. V. Efimov, O. A. Kolosova, A. V. Filippov and V. V. Klochkov, High-resolution NMR structure of the antimicrobial peptide protegrin-2 in the presence of DPC micelles, *J. Biomol. NMR*, 2015, **61**, 227–234.

51 K. S. Usachev, A. V. Filippov, E. A. Filippova, O. N. Antzutkin and V. V. Klochkov, Solution structures of Alzheimer's amyloid Aβ13-23 peptide: NMR studies in solution and in SDS, *J. Mol. Struct.*, 2013, **1049**, 436–440.

52 Q. Fei, D. Kent, W. M. Botello-Smith, F. Nur, S. Nur, A. Alsamarah, P. Chatterjee, M. Lambros and Y. Luo, Molecular Mechanism of Resveratrol's Lipid Membrane Protection, *Sci. Rep.*, 2018, **8**, 1–12.

53 C. Bonechi, S. Martini, L. Ciani, S. Lamponi, H. Rebmann, C. Rossi and S. Ristori, Using Liposomes as Carriers for Polyphenolic Compounds: The Case of Trans-Resveratrol, *PLoS One*, 2012, **7**, e41438.

54 T. W. Sirk, E. F. Brown, A. K. Sum and M. Friedman, Molecular dynamics study on the biophysical interactions of seven green tea catechins with lipid bilayers of cell membranes, *J. Agric. Food Chem.*, 2008, **56**, 7750–7758.